Nuclear Instruments and Methods in Physics Research A 1079 (2025) 170612

Contents lists available at ScienceDirect

Nuclear Inst. and Methods in Physics Research, A

journal homepage: www.elsevier.com/locate/nima

Full Length Article

New measurements of light yield quenching in EJ-200 and LYSO scintillators

A. Lega [a,b], R. Nicolaidis [a,b], F. Nozzoli [a,b,*], F. Dimiccoli [a,b], F.M. Follega [a,b], L.E. Ghezzer [a,b], R. Iuppa [a,b], E. Ricci [a,b], E. Verroi [a], P. Zuccon [a,b]

[a] *INFN, Trento Institute for Fundamental Physics and Applications, via Sommarive 14, 38123 Trento, Italy*
[b] *Physics Department, Trento University, via Sommarive 14, 38123 Trento, Italy*

ARTICLE INFO

Keywords:
Scintillation quenching
LYSO
Plastic scintillator

ABSTRACT

Lutetium–Yttrium OxyorthoSilicate (LYSO) crystals and EJ-200 plastic are widely recognized fast scintillators, valued for their high light output and robust mechanical properties, which make them well-suited for high-energy physics and space applications. The non-proportional light response of these scintillators, alongside their non-linear behavior at low-energy X-rays, has been extensively studied. Nevertheless, discrepancies in published measurements of light yield quenching remain unresolved. This study provides new insights by measuring light quenching in both scintillators under charged particle excitation and analyzing the non-linear response of LYSO to X-ray and γ-ray sources. The results are interpreted using the modified Birks–Onsager model, offering a reasonable description for the observed scintillation quenching phenomena.

1. Introduction

The non-proportional light response of organic and inorganic scintillators, especially when particle energy is deposited at high ionization densities, has been well-documented for decades [1]. This effect significantly contributes to light yield quenching when the scintillators are detecting slow charged particles or nuclei. Additionally, scintillation quenching leads to a loss of linearity in the scintillator response when irradiated by low-energy X/γ rays, primarily due to the low velocity of the ejected electrons. Moreover, the quenching effect plays a critical role in applications such as detecting fast neutron-induced nuclear recoils and in Dark Matter searches.

A simplified phenomenological model of scintillation quenching describes the interactions between charged carriers (electrons and holes, which primarily recombine non-radiatively) and neutral carriers (excitons, highly mobile bound states of electrons and holes that can transfer energy to luminescent centers).

The model considers the interplay of two concurring effects [2]. At high excitation densities, exciton-exciton interactions transfer part of their energy to phonons, i.e. without scintillation. This mechanism, first described by Birks [1] and later refined in [3], provides a model for the loss of luminous efficiency L_B as a function of the linear ionization density (dE/dx):

$$L_B = \eta_H + \frac{1-\eta_H}{1 + B\left(1-\eta_H\right)\frac{dE}{dx}} \tag{1}$$

where B is the Birk's parameter, setting the typical dE/dx scale at which quenching effects become significant. η_H represents the saturation value of luminous efficiency (its minimum value) and is interpreted in [3] as the fraction of carriers escaping from the high-ionization-density region near the track core to a surrounding halo region with lower ionization density.

A second mechanism plays an important role in modeling luminous efficiency at low ionization densities [4–7]. In particular, with $\eta_{e/h}$ representing the initial fraction of electrons and holes that do not form excitons, some electrons and holes may still recombine to form new excitons if they are within the Onsager radius. Therefore, thanks to this mechanism, an increase in the number of excitons is expected when the ionization density increases. The relative luminous efficiency L_O provided by this phenomenon is modeled as:

$$L_O = 1 - \eta_{e/h}\, e^{-\frac{dE/dx}{(dE/dx)_0}} \tag{2}$$

where $(dE/dx)_0$ is the ionization density scale relevant for the Onsager mechanism. Within this simplified model, the relative light yield of the scintillators is proportional to the product $L_B L_O$, effectively describing the scintillator's response to electrons and ions as well as the loss of linearity in response to low-energy photons [8]. Despite its simplicity, this quenching model can also explain the temperature dependence of the scintillator response [9] and the degradation in energy resolution when detecting low-energy electrons and photons [10,11].

High ionization densities may also occur when a large number of ionizing particles are detected by the same scintillator, a complete

* Corresponding author at: INFN, Trento Institute for Fundamental Physics and Applications, via Sommarive 14, 38123 Trento, Italy.
E-mail address: Francesco.Nozzoli@infn.it (F. Nozzoli).

https://doi.org/10.1016/j.nima.2025.170612
Received 5 March 2025; Received in revised form 30 April 2025; Accepted 4 May 2025
Available online 21 May 2025
0168-9002/

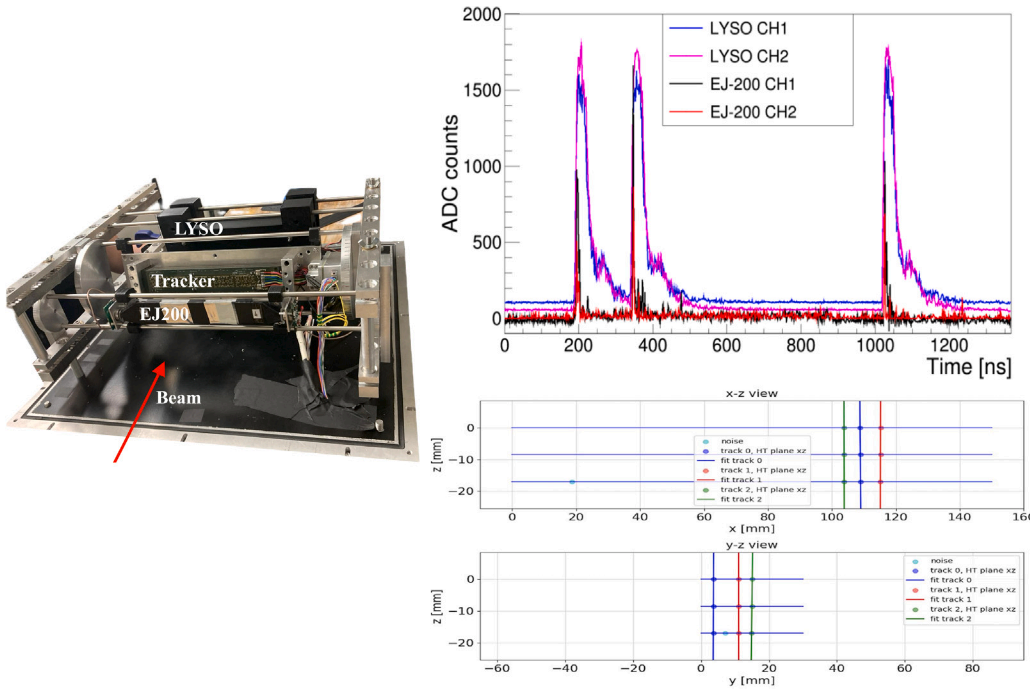

Fig. 1. Left: Experimental set-up used for the measurements. The trigger is provided by the EJ-200 plastic scintillator (15 × 3 × 0.2 cm^3). A signal in the EJ-200 triggers the digitization of a 3-layers ALTAI silicon pixel tracker and a LYSO:Ce scintillator (15 × 5 × 2.5 cm^3). Right: Event display showing an event with a pileup of three protons during high-rate (∼MHz) data acquisition. The upper part of the figure shows the PMT signals, while the lower part displays the side projections of the reconstructed tracks.

description of the detector's response should account for the quenching effects due to different particles crossing the same scintillator volume. In particular, this is responsible for the saturation effect observed in LYSO:Ce screens when used as electron beam monitors [12] or in sampling calorimeters detecting multi-TeV electromagnetic showers [13].

It is noteworthy that in these cases, all detected particles are minimally ionizing electrons; however, the simplified model based on quenching effects derived from the dE/dx of independently propagated particles fails.

Similarly, current Monte Carlo simulations may produce inaccurate evaluations of the scintillator response when accounting for the quenching effects of low-energy delta rays generated near the primary track, depending on the production/propagation thresholds.

2. Quenching measurements in EJ-200 and LYSO scintillators

Eljen Technology EJ-200 is a general purpose plastic scintillator (similar to Nuclear Enterprise's Pilot-F and Saint Gobain BC-408). It is based on polyvinyltoluene doped with proprietary wavelength-shifting fluors. Thanks to its high light output (10 ph./keV) long light attenuation length (3.8 m) and fast rise and decay times (0.9 ns and 2.1 ns respectively) EJ-200 is widely used in particle physics experiments. The Eljen Technology document library provides a plot illustrating the response of EJ-200 to charged particles with different ionization densities. Complementary data are available from the Scintillator Library at Lawrence Berkeley National Laboratory. These datasets [14] were obtained by analyzing EJ-200's signal under to electron recoils up to 1 MeV [15] and proton recoils up to a few MeV, induced by exposure to fast neutrons [16–18]. Additionally, the responses of EJ-200 to electrons [6] and γ-ray sources [19] were studied. The results, assuming the original Birks' law (i.e. imposing $n_H = 0$ and $\eta_{e/h} = 0$ in the generalized model) provide: $1/B = 91$ MeV/cm [6] and $B = 0.016$ cm/MeV [19], respectively. A recent investigation of EJ-200's response to relativistic nuclei [20] suggests that significant light yield quenching occurs only when dE/dx exceeds 100 MeV/cm. However, this result appears inconsistent with previous measurements.

The second scintillator investigated in this study is the Cerium doped LYSO (Lutetium–Yttrium OxyorthoSilicate) scintillator. LYSO:Ce is a high density (∼7.2 g/cm^3), high effective atomic number (Z_{eff} ∼65), high light yield (∼30 ph./keV) fast (τ ∼40 ns) inorganic scintillator. These characteristics, along with the good radiation hardness, relatively high mechanical strength and moderate cost, have made LYSO a widely adopted material for medical PET scanners and high energy particle detectors, despite its relatively high intrinsic radioactivity (∼40 Bq/g) [21]. Non proportionality to sub-MeV x/γ rays is a well-known property of LYSO [22–25].

Initial measurements of LYSO's response to protons [26,27] and nuclei [28,29] have determined scintillation quenching parameters using different modified Birks' formulations.

A recent study on LYSO's response to a 30 GeV/n relativistic Argon beam (and its fragments) provides detailed measurement of the generalized Birks–Onsager model parameters for this scintillator [2]. As with EJ-200, a quantitative comparison of previous LYSO measurements reveals discrepancies in the degree of scintillation quenching as a function of linear ionization density.

3. Measurement with x/γ, μ and particle beam

To evaluate the quenching effects in EJ-200 and LYSO scintillators, we implemented the set-up shown in Fig. 1.left.

The main trigger is provided by the EJ-200 plastic scintillator (15 × 3 × 0.2 cm^3). A signal in the EJ-200 triggers the digitization of a 3-layer ALTAI silicon pixel tracker [30] and a LYSO:Ce scintillator (15 × 5 × 2.5 cm^3, 1350 g, produced by Filar Optomaterials). The light produced by the scintillators was collected coupling both sides of the detectors with Hamamatsu R9880U-210 PhotoMultipliers (PMTs) whose signal was sampled using a 5GS/s digitizer (DT5742, CAEN) to measure the peak amplitude. The high resolution (∼ 28 μm pitch) silicon tracker allows measurement of the particle direction and identification (and, if necessary, rejection) of events where a pileup of multiple particles occurs. Fig. 1.right, shows an example of an event acquired during an high (∼MHz) rate, 120 MeV, proton beam. In this case,

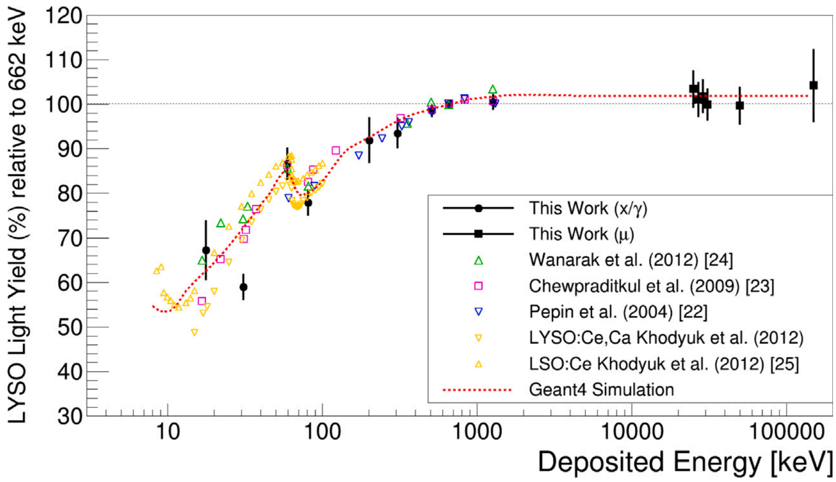

Fig. 2. Comparison of calibrations collected for LYSO scintillators. Black squares represent muon calibrations obtained by aligning the three sides of the detector vertically. Black circles represent calibrations with x/γ ray sources: ^{241}Am (17.8 keV, 59.5 keV), ^{133}Ba (30.8 keV, 81 keV), ^{176}Lu (202 keV, 307 keV) and ^{22}Na (511 keV, 1275 keV). The drop in relative light yield for x/γ rays below 1 MeV is consistent with the behavior measured in [22–25] and can be simulated using the generalized quenching model with parameters: $1/B$ = 11.5 MeV/cm, η_H = 0.027, $\eta_{e/h}$ = 0.75 and $(dE/dx)_0$ = 145 MeV/cm (red dashed line).

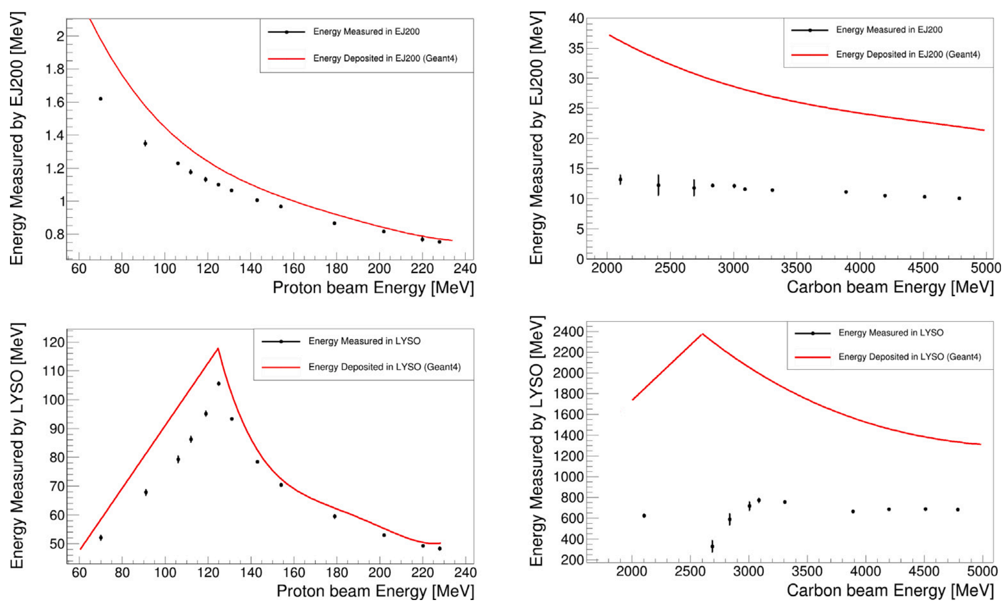

Fig. 3. Energy deposition as measured by different scintillators (black points) as a function of beam energy. The red lines represent the energy deposition evaluated using Geant4 simulations. The top plots correspond to EJ-200 while bottom plots correspond to LYSO scintillators. Only protons with energies above 125 MeV and Carbon ions with energies above 2600 MeV were able to fully traverse 2.5 cm of LYSO. The ratio between measured and deposited energy decreases as particle energy decreases or particle charge increases, as a consequence of scintillation quenching.

the two scintillators (top panel) detect the energy depositions of three different protons identified by theirs tracks in the silicon tracker.

The scintillators were calibrated using the known energy deposited by (vertical and inclined) cosmic muons. For the case of the LYSO, thanks to the high Z_{eff}, calibrations with x/γ rays are also feasible. Due to the intrinsic radioactivity of ^{176}Lu (54kBq/1350 g), all x/γ ray measurements below 662 keV were performed using a small (8 g) LYSO sample. Fig. 2 summarizes the calibrations collected for the LYSO scintillators. Black squared points represent the muon calibrations at deposited energies of 25–35 MeV, 50 MeV and 150 MeV, corresponding to muons crossing through the 2.5 cm (with different inclinations), 5 cm (vertically aligned) and 15 cm (vertically aligned) crystal sides. Black circles represents the calibrations with x/γ ray sources (^{241}Am, ^{133}Ba, ^{176}Lu, ^{22}Na). Fig. 2 also reports the LYSO response to x/γ rays from other measurements [22–25]. The observed non-linearity of the LYSO response to low energy x/γ rays can be modeled considering the scintillation light quenching of non-relativistic electrons emitted during photon energy deposition. The local drops of the light yield above ∼10 keV and above 63 keV are due to the relatively low energies of the electrons emitted in the photoelectric ionization of L edges and K edge of Lutetium which becomes energetically allowed channels. The red dashed line shown in Fig. 2 has been obtained from a Geant4 [31] simulation using the G4EmStandardPhysics_opt1 model for the electromagnetic physics processes and using the generalized quenching model with parameters: $1/B$ = 11.5 MeV/cm, η_H = 0.027, $\eta_{e/h}$ = 0.75 and $(dE/dx)_0$ = 145 MeV/cm (further details in the following sections).

During the measurements with particle beams, the detectors have been aligned to ensure that particles passed perpendicularly through 0.2 cm of EJ-200 and 2.5 cm of LYSO. The measurements with protons in the range 70–228 MeV were performed at the INFN/TIFPA experimental room of the APSS Protontherapy center in Trento [32]. At the CNAO (Pavia) center [33] the detector was also characterized with

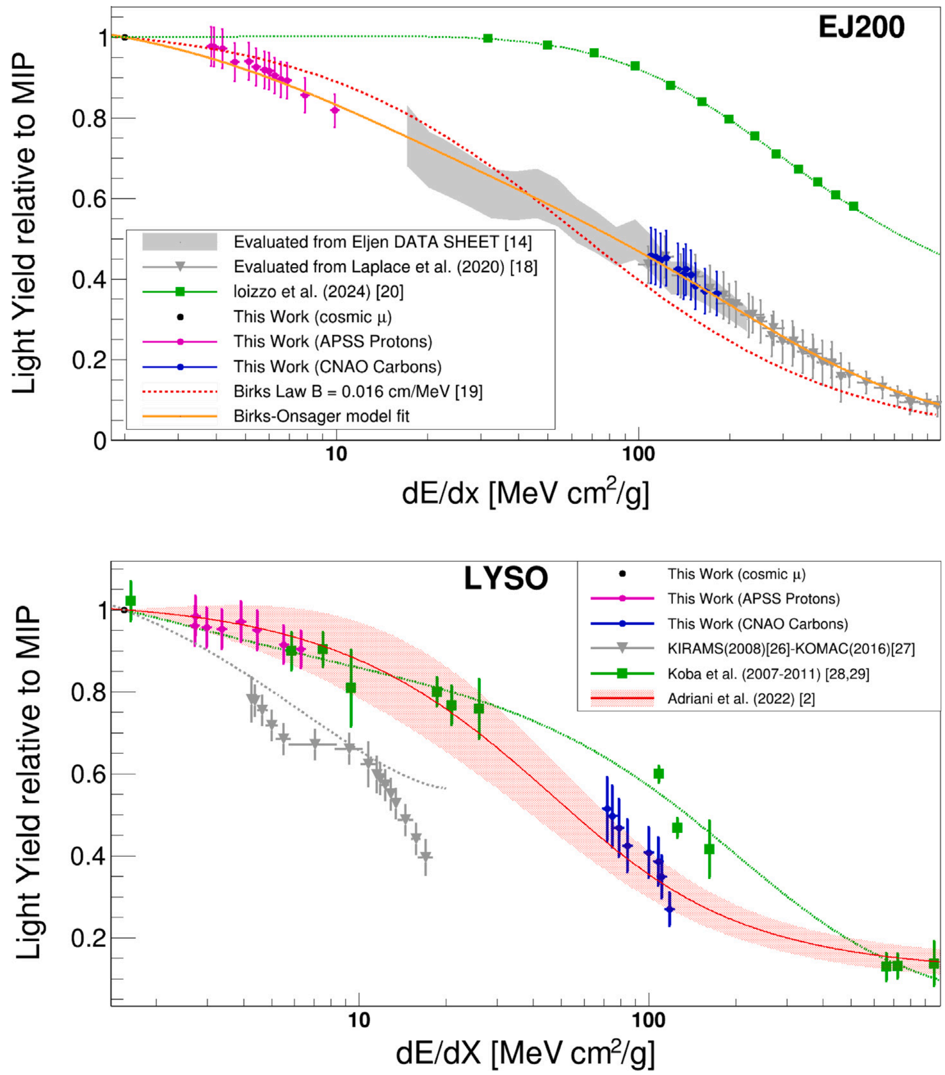

Fig. 4. Light yield relative to MIP (Minimum Ionizing Particles, μ black points) measured for EJ-200 (top plot) and LYSO (bottom plot) scintillators. Magenta and blue points represent measurements obtained with Protons and Carbon ions (APSS and CNAO beam), respectively, crossing the two scintillators. The EJ-200 measurements are compared with the results from [14,18,20] and with the pure Birks Law, B = 0.016 cm/MeV, as in [19] (red dashed line). The orange line is the Birks–Onsager best fit (excluding [20]) with parameters: 1/B = 12.0 ± 1.3 MeV/cm, $\eta_{e/h}$ = 0.853 ± 0.014, $(dE/dx)_0$ = 134 ± 6 MeV/cm, while η_H, which is consistent with zero, was fixed at 0. The LYSO measurements are compared with the results from [26–29] and with the Birks–Onsager model (1/B = 45.1 ± 9.1 MeV/cm, η_H = 0.0274 ± 0.0048, $\eta_{e/h}$ = 0.758 ± 0.045 and $(dE/dx)_0$ = 164.7 ± 8.4 MeV/cm; red line with filled band) as suggested in [2].

170–400 MeV/n Carbons and with 110–130 MeV protons. Monte Carlo simulations were performed using Geant4 [31] to evaluate the expected energy deposition and track length distributions for each beam energy.

Fig. 3 shows the energy deposition as measured by EJ-200 and LYSO scintillators (black points) as a function of the beam energy; the red lines represent the energy depositions as evaluated from the Geant4 simulation. Only protons with energies above 125 MeV and Carbon with energies above 2600 MeV were able to cross the whole 2.5 cm of LYSO. The ratio between measured and expected deposited energy decreases as particle energy decreases or particle charge increases; this behavior is a consequence of the scintillation quenching. In particular, for the Carbon beam (lower-right plot of Fig. 3), a counterintuitive behavior is observed below 3 GeV: as a result of an increasing deposited energy in the LYSO crystal, the scintillation light sharply decreases.[1]

Fig. 4 summarizes the Light Yield relative to the MIP (Minimum Ionizing Particles, μ black points) measured for EJ-200 (top plot) and for LYSO (bottom plot) scintillators. Magenta/blue points are our measurements obtained with Protons/Carbons crossing the two scintillators (APSS and CNAO beam respectively); The dE/dx quantity has been derived from Geant4 simulations, representing the average specific ionization density expected for each beam energy. The other points in Fig. 4 are from the light yield measurements existing in literature for EJ-200 and LYSO.

In particular, in [14,18] the EJ-200 light response as a function of the particle energy is provided only for stopping particles. Therefore, to evaluate the gray filled band and gray triangles in top plot of Fig. 4 the derivative of the light response was performed and the average specific energy loss within the differentiation energy interval was considered. Same procedure was adopted to analyze the results of [26,27] plotted as gray triangles in the bottom panel of Fig. 4, along with the quadratic modified Birks model considered in [27] (gray dashed line).

4. Discussion and conclusions

Our new measurements of scintillation light quenching in EJ-200 are consistent with the expectations derived from [14,18] and roughly

[1] This behavior is similar to the 'smoke-ring' effect observed in [12], where a doughnut-shaped light profile is emitted from LYSO screens used as high-intensity beam monitors.

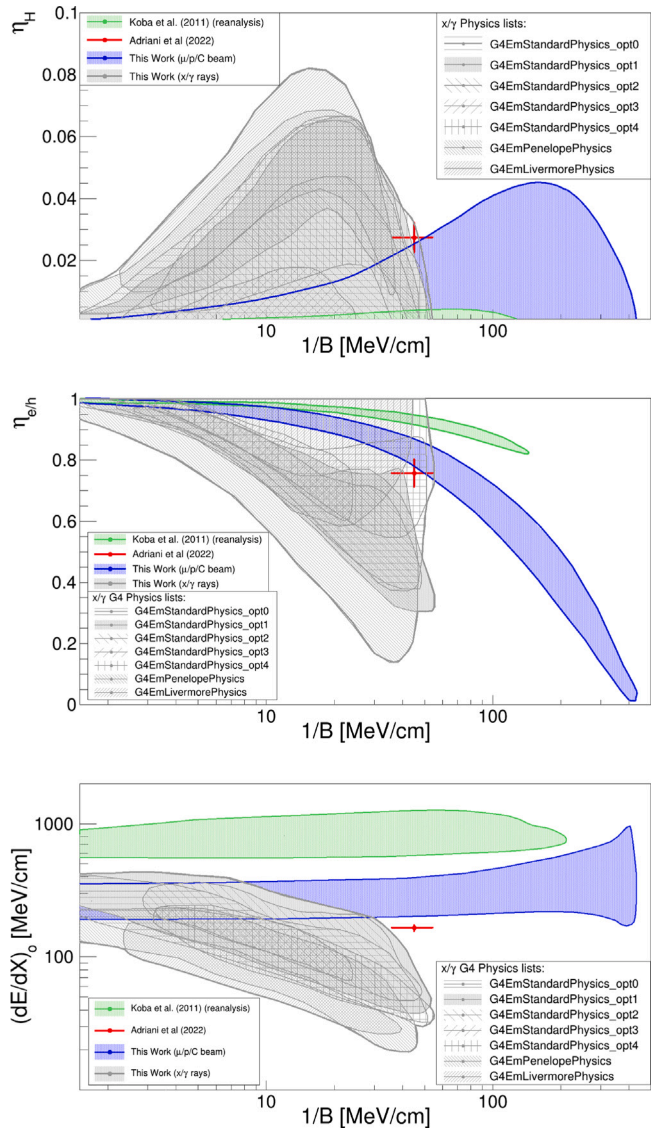

Fig. 5. Configurations allowed at 1σ C.L. for the parameters of the Birks–Onsager quenching model of the LYSO scintillator. The gray region is the superposition of the 1σ allowed configurations based on the analysis of the non-linearity to low energy x/γ rays using G4EmStandardPhysics_opt0 to _opt4, G4EmPenelopePhysics and G4EmLivermorePhysics models.

follow the pure Birks model suggested in [19]. However, the light quenching measurements reported in [20] (green squares and dotted line in the top plot of Fig. 4) shows significant discrepancies compared to the other results. Further investigation is required to determine whether the readout used in [20] detects Cherenkov light or scintillation components of EJ-200 that are less affected by quenching effects. Excluding the data from [20], a fit using the Birks–Onsager model for EJ-200 data (orange line) yields the following parameters: 1/B = 12.0 ± 1.3 MeV/cm, $\eta_{e/h}$ = 0.853 ± 0.014, $(dE/dx)_0$ = 134 ± 6 MeV/cm, while η_H, which is consistent with zero, was fixed at 0.

Our new measurements of the scintillation light quenching in LYSO agree with those reported by Adriani et al. [2]. The results of [26,27] (gray triangles) are not consistent with the others, however, they quotes a unusually low density (5.37 g/cm^3) for their LYSO crystal. A more detailed analysis of LYSO scintillation quenching was performed, incorporating the non-linearity in response to x/γ rays (as shown in Fig. 2) within the framework of the Birks–Onsager model. In particular, within the Geant4 simulation framework, for each charged particle step, the scintillation light efficiency was evaluated as a function of the computed dE/dx.

We conducted a grid scan of Geant4 simulation results, varying the four quenching parameters <B, η_H, $\eta_{e/h}$, $(dE/dx)_0$> to evaluate the expected LYSO scintillator response to mono-energetic photons. This allowed fitting the x/γ rays measurements in Fig. 2 using the Birks–Onsager quenching model (red dashed line).

To ensure an accurate simulation of low-energy atomic processes, the production cuts for all particles were lowered to 10 nm, and the threshold for production cut tables was reduced to 100 eV (the lowest value currently allowed by the Geant4 Electromagnetic Physics lists). These settings required a considerable computational effort to perform the simulations.

To evaluate the systematic effects related to the choice of the Geant4 description of the low energy EM processes, six different simulations were performed for each configuration, using G4EmStandardPhysics_opt0 to _opt4, G4EmPenelopePhysics and G4EmLivermorePhysics models.

The Birks–Onsager quenching model parameter values allowed at 1σ confidence level (C.L.) for the LYSO are shown in Fig. 5. The gray filled region is the superposition of the allowed configurations based on the analysis of the LYSO non-linearity to low energy x/γ rays. Fig. 5 also shows the parameter allowed regions obtained from our Proton/Carbon test beam measurements (blue) and those (green) obtained from a re-analysis, in terms of the Birks–Onsager model, of the Koba et al. [28,29] measurements (lower panel of Fig. 4).

A comparison between our x/γ/μ/p/C measurements and the results of Adriani et al. [2] (single red point in Fig. 5) shows a reasonable agreement. Notably, current Geant4 simulations, despite their computational demands, successfully describe the non-linearity in the LYSO response to low energy x/γ rays in terms of the Birks–Onsager quenching of the produced electrons.

When comparing with the results from Koba et al. [28,29], we observe a significant disagreement on the $(dE/dx)_0$ parameter (see Fig. 5 bottom panel). This suggests that their measurements may overestimate the LYSO light yield by a factor ∼3/2 in the 100–150 MeV cm^2/g range (explored by their Carbon beam).

In conclusion, our study provides a precise measurement of the Birks–Onsager model parameters for EJ-200 scintillators and confirms the results of Adriani et al. [2] for the light quenching of the LYSO crystals.

CRediT authorship contribution statement

A. Lega: Writing – original draft, Validation, Software, Methodology, Investigation, Formal analysis, Data curation, Conceptualization. **R. Nicolaidis:** Writing – original draft, Visualization, Validation, Software, Methodology, Investigation, Formal analysis, Data curation. **F. Nozzoli:** Writing – review & editing, Writing – original draft, Visualization, Validation, Supervision, Software, Methodology, Investigation, Formal analysis, Data curation, Conceptualization. **F. Dimiccoli:** Writing – review & editing, Supervision, Formal analysis. **F.M. Follega:** Writing – review & editing, Supervision, Formal analysis. **L.E. Ghezzer:** Visualization, Investigation, Data curation. **R. Iuppa:** Writing – review & editing, Visualization, Validation, Supervision, Methodology, Investigation, Formal analysis, Data curation, Conceptualization. **E. Ricci:** Writing – review & editing, Visualization, Validation, Supervision, Methodology, Investigation, Formal analysis, Data curation, Conceptualization. **E. Verroi:** Visualization, Supervision, Investigation, Data curation. **P. Zuccon:** Writing – review & editing, Visualization, Validation, Supervision, Investigation, Formal analysis, Conceptualization.

Declaration of competing interest

The authors declare that they have no known competing financial interests or personal relationships that could have appeared to influence the work reported in this paper.

Data availability

Data will be made available on request.

References

[1] J.B. Birks, The Theory and Practice of Scintillation Counting: International Series of Monographs in Electronics and Instrumentation, vol. 27, Elsevier, 2013.

[2] O. Adriani, E. Berti, P. Betti, G. Bigongiari, L. Bonechi, M. Bongi, S. Bottai, P. Brogi, G. Castellini, C. Checchia, et al., Light yield non-proportionality of inorganic crystals and its effect on cosmic-ray measurements, J. Instrum. 17 (08) (2022) P08014, http://dx.doi.org/10.1088/1748-0221/17/08/P08014.

[3] G. Tarle, S.P. Ahlen, B.G. Cartwright, Cosmic ray isotope abundances from chromium to nickel, ApJ 230 (1979) 607–620, http://dx.doi.org/10.1086/157119.

[4] W.W. Moses, S.A. Payne, W.-S. Choong, G. Hull, B.W. Reutter, Scintillator non-proportionality: Present understanding and future challenges, IEEE Trans. Nucl. Sci. 55 (3) (2008) 1049–1053, http://dx.doi.org/10.1109/TNS.2008.922802.

[5] S.A. Payne, N.J. Cherepy, G. Hull, J.D. Valentine, W.W. Moses, W.-S. Choong, Nonproportionality of scintillator detectors: Theory and experiment, IEEE Trans. Nucl. Sci. 56 (4) (2009) 2506–2512, http://dx.doi.org/10.1109/TNS.2009.2023657.

[6] S.A. Payne, W.W. Moses, S. Sheets, L. Ahle, N.J. Cherepy, B. Sturm, S. Dazeley, G. Bizarri, W.-S. Choong, Nonproportionality of scintillator detectors: Theory and experiment. II, IEEE Trans. Nucl. Sci. 58 (6) (2011) 3392–3402, http://dx.doi.org/10.1109/TNS.2011.2167687.

[7] S. Payne, S. Hunter, B. Sturm, N. Cherepy, L. Ahle, S. Sheets, S. Dazeley, W. Moses, G. Bizarri, Physics of scintillator nonproportionality, in: Hard X-Ray, Gamma-Ray, and Neutron Detector Physics XIII, vol. 8142, SPIE, 2011, pp. 251–257.

[8] P.R. Beck, S.A. Payne, S. Hunter, L. Ahle, N.J. Cherepy, E.L. Swanberg, Non-proportionality of scintillator detectors. V. Comparing the Gamma and electron response, IEEE Trans. Nucl. Sci. 62 (3) (2015) 1429–1436, http://dx.doi.org/10.1109/TNS.2015.2414357.

[9] S.A. Payne, S. Hunter, L. Ahle, N.J. Cherepy, E. Swanberg, Nonproportionality of scintillator detectors. III. Temperature dependence studies, IEEE Trans. Nucl. Sci. 61 (5) (2014) 2771–2777, http://dx.doi.org/10.1109/TNS.2014.2343572.

[10] P. Iredale, The effect of the non-proportional response of NaI(Tl) crystals to electrons upon the resolution for γ-rays, Nucl. Instrum. Methods 11 (1961) 340–346, http://dx.doi.org/10.1016/0029-554X(61)90036-2.

[11] S.A. Payne, Nonproportionality of scintillator detectors. IV. Resolution contribution from Delta-rays, IEEE Trans. Nucl. Sci. 62 (1) (2015) 372–380, http://dx.doi.org/10.1109/TNS.2014.2387256.

[12] G. Kube, S. Liu, A. Novokshonov, M. Scholz, Identification and mitigation of smoke-ring effects in scintillator-based electron beam images at the European XFEL, in: Proc. FEL'19, in: Free Electron Laser Conference, (39) JACoW Publishing, Geneva, Switzerland, 2019, pp. 301–306, http://dx.doi.org/10.18429/JACoW-FEL2019-WEB01.

[13] A. Kounine, Z. Weng, W. Xu, C. Zhang, Precision measurement of 0.5GeV–3TeV electrons and positrons using the AMS electromagnetic calorimeter, Nucl. Instrum. Meth. Phys. Res. Sect. A: Accel. Spectrometers Detect. Assoc. Equip. 869 (2017) 110–117, http://dx.doi.org/10.1016/j.nima.2017.07.013.

[14] Eljen technology: Response of EJ-200 plastic scintillator and Berkeley national laboratory scintillator library, 2025, https://eljentechnology.com/images/technical_library/EJ200_Resp.pdf, https://scintillator.lbl.gov/ej-200-bc-408-pilot-f-quenching-data. (Accessed 10 April 2025).

[15] L. Swiderski, R. Marcinkowski, M. Moszynski, W. Czarnacki, M. Szawlowski, T. Szczesniak, G. Pausch, C. Plettner, K. Roemer, Electron response of some low-Z scintillators in wide energy range, J. Instrum. 7 (06) (2012) P06011, http://dx.doi.org/10.1088/1748-0221/7/06/P06011.

[16] T. Langford, E. Beise, H. Breuer, C. Heimbach, G. Ji, J. Nico, Development and characterization of a high sensitivity segmented fast neutron spectrometer (FaNS-2), J. Instrum. 11 (01) (2016) P01006, http://dx.doi.org/10.1088/1748-0221/11/01/P01006.

[17] A. Tkaczyk, H. Saare, C. Ipbüker, F. Schulte, P. Mastinu, J. Paepen, B. Pedersen, P. Schillebeeckx, G. Varasano, Characterization of EJ-200 plastic scintillators as active background shield for cosmogenic radiation, Nucl. Instrum. Meth. Phys. Res. Sect. A: Accel. SpectrometersDetect. Assoc. Equip. 882 (2018) 96–104, http://dx.doi.org/10.1016/j.nima.2017.10.088.

[18] T. Laplace, B. Goldblum, J. Brown, D. Bleuel, C. Brand, G. Gabella, T. Jordan, C. Moore, N. Munshi, Z. Sweger, A. Sweet, E. Brubaker, Low energy light yield of fast plastic scintillators, Nucl. Instrum. Meth. Phys. Res. Sect. A: Accel. SpectrometersDetect. Assoc. Equip. 954 (2020) 161444, http://dx.doi.org/10.1016/j.nima.2018.10.122, Symposium on Radiation Measurements and Applications XVII.

[19] S.M. Tajudin, Y. Namito, T. Sanami, H. Hirayama, Response of plastic scintillator to gamma sources, Appl. Radiat. Isot. 159 (2020) 109086, http://dx.doi.org/10.1016/j.apradiso.2020.109086.

[20] P. Loizzo, D. Cerasole, F. Barbato, E. Bissaldi, I. Cagnoli, E. Casilli, I. De Mitri, F. De Palma, A. Di Giovanni, L. Di Venere, G. Fontanella, P. Fusco, F. Gargano, E. Ghose, M. Mazziotta, R. Pillera, D. Serini, L. Silveri, Characterization of light yield non-proportionality in plastic scintillator-based detectors for satellite cosmic-ray experiments, Nucl. Instrum. Meth. Phys. Res. Sect. A: Accel. SpectrometersDetect. Assoc. Equip. 1069 (2024) 169888, http://dx.doi.org/10.1016/j.nima.2024.169888.

[21] L.E. Ghezzer, F. Nozzoli, R. Nicolaidis, C. De Santis, R. Iuppa, P. Zuccon, Search for electron capture in Lu176 with a lutetium yttrium oxyorthosilicate scintillator, Phys. Rev. C 107 (4) (2023) 045504, http://dx.doi.org/10.1103/PhysRevC.107.045504.

[22] C. Pepin, P. Berard, A.-L. Perrot, C. Pepin, D. Houde, R. Lecomte, C. Melcher, H. Dautet, Properties of LYSO and recent LSO scintillators for phoswich PET detectors, IEEE Trans. Nucl. Sci. 51 (3) (2004) 789–795, http://dx.doi.org/10.1109/TNS.2004.829781.

[23] W. Chewpraditkul, L. Swiderski, M. Moszynski, T. Szczesniak, A. Syntfeld-Kazuch, C. Wanarak, P. Limsuwan, Scintillation properties of $\mathrm{LuAG:Ce}$, $\mathrm{YAG:Ce}$ and $\mathrm{LYSO:Ce}$ crystals for Gamma-ray detection, IEEE Trans. Nucl. Sci. 56 (6) (2009) 3800–3805, http://dx.doi.org/10.1109/TNS.2009.2033994.

[24] C. Wanarak, W. Chewpraditkul, A. Phunpueok, Light yield non-proportionality and energy resolution of $\mathrm{Lu_{1.95}Y_{0.05}SiO_5:Ce}$ and $\mathrm{Lu_2SiO_5:Ce}$ scintillation crystals, Procedia Eng. 32 (2012) 765–771, http://dx.doi.org/10.1016/j.proeng.2012.02.010, ISEEC.

[25] I.V. Khodyuk, P. Dorenbos, Trends and patterns of scintillator nonproportionality, IEEE Trans. Nucl. Sci. 59 (6) (2012) 3320–3331, http://dx.doi.org/10.1109/TNS.2012.2221094.

[26] J. So, H. Kim, H. Kang, H. Park, S. Lee, S. Kim, K. Kim, M. Lee, The proton energy response of a LYSO crystal, J. Korean Phys. Soc. 52 (3) (2008) 925–929, http://dx.doi.org/10.3938/jkps.52.925.

[27] J.K. Sang, K. MinJeong, P. Jeongmin, L. Jooyoung, S. Jukyung, H. DaeHoon, H. Yongseok, Measurement of the proton luminescence response and determination of the birks parameters of the LYSO crystal, New Phys.: Sae Mulli 66 (6) (2016) 679–684, http://dx.doi.org/10.3938/NPSM.66.679.

[28] Y. Koba, G. Wakabayashi, M. Imamura, Y. Uozumi, N. Koba, H. Iwamoto, H. Ohkawa, T. Shimazu, N. Matsufuji, P. Evtoukhovitch, V. Kalinnikov, N. Khomutov, N. Kuchinskii, A. Moiseenko, D. Mzavia, V. Samoilov, Z. Tsamalaidze, Light output response of LYSO(Ce) crystal to relativistic helium and carbon ions, in: 2007 IEEE Nuclear Science Symposium Conference Record, vol. 3, 2007, pp. 2303–2306, http://dx.doi.org/10.1109/NSSMIC.2007.4436606.

[29] Y. Koba, H. Iwamoto, K. Kiyohara, T. Nagasaki, G. Wakabayashi, Y. Uozumi, N. Matsufuji, Scintillation efficiency of inorganic scintillators for intermediate-energy charged particles, Prog. Nucl. Sci. Technol. 1 (2011) 218–221, http://dx.doi.org/10.15669/PNST.1.218.

[30] E. Ricci, First use of monolithic active pixel sensors for tracking particles in space, in: 44th COSPAR Scientific Assembly. Held 16-24 July 44, 44, 2022, p. 3057.

[31] J. Allison, K. Amako, J. Apostolakis, P. Arce, M. Asai, T. Aso, E. Bagli, A. Bagulya, S. Banerjee, G. Barrand, B. Beck, A. Bogdanov, D. Brandt, J. Brown, H. Burkhardt, P. Canal, D. Cano-Ott, S. Chauvie, K. Cho, G. Cirrone, G. Cooperman, M. Cortés-Giraldo, G. Cosmo, G. Cuttone, G. Depaola, L. Desorgher, X. Dong, A. Dotti, V. Elvira, G. Folger, Z. Francis, A. Galoyan, L. Garnier, M. Gayer, K. Genser, V. Grichine, S. Guatelli, P. Guèye, P. Gumplinger, A. Howard, I. Hřivnáčová, S. Hwang, S. Incerti, A. Ivanchenko, V. Ivanchenko, F. Jones, S. Jun, P. Kaitaniemi, N. Karakatsanis, M. Karamitros, M. Kelsey, A. Kimura, T. Koi, H. Kurashige, A. Lechner, S. Lee, F. Longo, M. Maire, D. Mancusi, A. Mantero, E. Mendoza, B. Morgan, K. Murakami, T. Nikitina, L. Pandola, P. Paprocki, J. Perl, I. Petrović, M. Pia, W. Pokorski, J. Quesada, M. Raine, M. Reis, A. Ribon, A. Ristić Fira, F. Romano, G. Russo, G. Santin, T. Sasaki, D. Sawkey, J. Shin, I. Strakovsky, A. Taborda, S. Tanaka, B. Tomé, T. Toshito, H. Tran, P. Truscott, L. Urban, V. Uzhinsky, J. Verbeke, M. Verderi, B. Wendt, H. Wenzel, D. Wright, D. Wright, T. Yamashita, J. Yarba, H. Yoshida, Recent developments in Geant4, Nucl. Instrum. Meth. Phys. Res. Sect. A: Accel. SpectrometersDetect. Assoc. Equip. 835 (2016) 186–225, http://dx.doi.org/10.1016/j.nima.2016.06.125.

[32] F. Tommasino, M. Rovituso, S. Fabiano, S. Piffer, C. Manea, S. Lorentini, S. Lanzone, Z. Wang, M. Pasini, W. Burger, C. La Tessa, E. Scifoni, M. Schwarz, M. Durante, Proton beam characterization in the experimental room of the Trento Proton Therapy facility, Nucl. Instrum. Meth. Phys. Res. Sect. A: Accel. Spectrometers Detect. Assoc. Equip. 869 (2017) 15–20, http://dx.doi.org/10.1016/j.nima.2017.06.017.

[33] S. Giordanengo, M.A. Garella, F. Marchetto, F. Bourhaleb, M. Ciocca, A. Mirandola, V. Monaco, M.A. Hosseini, C. Peroni, R. Sacchi, R. Cirio, M. Donetti, The CNAO dose delivery system for modulated scanning ion beam radiotherapy, Med. Phys. 42 (1) 263–275, http://dx.doi.org/10.1118/1.4903276.